Mechanical Strength, Thermal Stability, and Hydrophobicity of Fiber Materials after Removal of Residual Lignin

Quanliang Wang,[a] Shengling Xiao,[a,*] Sheldon Q. Shi,[b] and Liping Cai [b]

The behaviors of the mechanical, hydrophobic, and thermal properties of the molded fiber product (MFP) were examined after the removal of residual lignin. The fibers resulting from the chemi-thermomechanical pulping and bleaching processes were treated by extended delignification, namely by their reaction with glacial acetic acid and sodium chlorite. The changes in surface composition, chemical structure, crystallinity, microstructure, and thermal stability of the MFP were investigated by X-ray photoelectron spectroscopy (XPS), Fourier transform infrared (FTIR) spectroscopy, X-ray diffraction (XRD), scanning electron microscopy (SEM), and thermogravimetric analysis (TGA), respectively. Results showed that the composition and structure of carbohydrates on the fiber surface were not changed significantly, the lignin in fibers was almost completely removed, the relative content of intermolecular hydrogen bonds in cellulose and the contact area between fibers was increased, and the crystallinity index increased from 79.5% to 81.4% after the extended delignification. When the content of lignin decreased from 5.78% to 0.02%, the tensile strength of the MFP increased 25.6%, but little changes were found in the bending strength. The onset thermal decomposition temperature of MFP increased from 242 °C to 250 °C and the maximum rate of degradation temperature increased from 347 °C to 350 °C.

Keywords: Extended delignification; Molded fiber materials; Mechanical property; Thermal stability; Hydrophobic

*Contact information: a: College of Engineering and Technology, Northeast Forestry University, 26 Hexing Road, Harbin 150040, China; b: Department of Mechanical and Energy Engineering, University of North Texas, Denton, TX 76203, USA; *Corresponding author: shenglingxiao@126.com*

INTRODUCTION

The molded fiber product (MFP) has developed rapidly in recent years because it can be a good substitute for plastic and solid wood materials. Because of its powerful three-dimensional molding capacity, excellent mechanical properties, and great potential for modification, MFP has a very broad application prospect in the packaging, medical, and high-end fields such as automobile manufacturing (Gällstedt and Hedenqvist 2006; Obradovic *et al*. 2014). Traditional molded fiber materials are usually molded by single suction molding with a density of 0.22 g•cm^{-3} to 0.33 g•cm^{-3} and are usually used for packing small and light products (Yang *et al*. 2005). However, MFP with a density of 0.8 g•cm^{-3} to 1.1 g•cm^{-3} are molded by a special molding process using plant fiber pulps as the raw materials, which can meet the requirements of large structures and have high load bearing capacities (Wang *et al*. 2017).

Traditional fiber molding materials are mainly made from chemical pulp fibers. These fiber surfaces are covered with carbohydrates that expose a multitude of hydroxyl groups. These groups are beneficial to forming high-strength bonds between fibers (Cho *et al*. 2009). However, lignin on the fiber surface will be removed as much as possible in pulping due to its lower content of active groups and higher steric hindrance (Zhang *et al.* 2013). Therefore, the fiber molding materials use pulp fibers with small amounts of residual lignin within fibers as the raw material. In general, there is a comprehensive requirement for the mechanical properties of MFP, especially for tensile strength and bending strength. The tensile strength is directly related to the inter-fiber bond strength while the bending strength is closely related to fiber stiffness, material density, *etc*. (Korai *et al*. 2015; Miletzky *et al*. 2015). The removal of residual lignin within fibers may have little effect on the fiber surface chemical composition, but it is closely related to the fiber hardness and its internal structure. Lignin, with its three-dimensional network structure, acts as a filling agent in cellulose fibers and the removal of residual lignin makes the internal structure of fibers looser. This looseness is beneficial to the softening and deformation of fibers (Ferrer *et al*. 2012; Nair and Yan 2015). Obviously, these have important effects on the material's physical characteristics, such as inter-fiber bonding area, material density, *etc*., which can make the material exhibit different mechanical properties (especially for bending strength).

At the same time, natural lignin is a hydrophobic polymer and has a wider range of thermal degradation than carbohydrates, which may cause the fiber material to show different thermal and hydrophobic properties due to the removal of residual lignin (Poletto *et al*. 2012; Rojo *et al*. 2015). Generally, the hydrophobic natural lignin will introduce hydrophilic groups in the process of delignification, which can change the material surface hydrophobicity (Kadla and Chang 2002). The higher degradation temperature range of lignin is due to the different thermal stabilities of several oxygen related functional groups in its structure, and extended delignification may cause changes in the material thermal properties while causing changes in the fiber composition (Domínguez *et al*. 2008; Brebu *et al*. 2013; Laurichesse and Avérous 2014).

Extended delignification refers to the removal of residual lignin within pulp fibers by chemical means *via* reduced carbohydrates loss. The aim is to reduce the steric hindrance of carbohydrates during their reaction and improve the properties of fibers and their molding materials by decreasing fiber softness and increasing fiber whiteness (Baptista *et al*. 2008; Wen *et al*. 2013). Extended delignification does not cause an obvious change in the tensile strength of individual fibers (Zhang *et al*. 2012). However, there is a meaningful linear relationship between the lignin content in fibers and the tensile strength of paper (Lin *et al*. 2011). It can be seen that there is no direct relationship between the mechanical properties of a final material and the strength of its individual fibers. The mechanical strength of fiber materials is determined by factors such as fiber stiffness, inter-fiber bond strength, material density, *etc*. Therefore, the study of the impact of extended delignification on the product is much more practical than that of the individual fibers. However, the specific impact of extended delignification on fiber molding product properties has not yet been reported. It is of great significance to study the effects of the removal of residual lignin on the mechanical, hydrophobic, and thermal properties of MFP.

In this study, pulp fibers containing small amounts of residual lignin were used as the raw material, and fibers with almost no residual lignin were obtained by extended delignification using sodium chlorite. Two kinds of pulp fibers were used separately for

the preparation of MFP by a hot-press molding process to investigate the effect of the removal of residual lignin on the mechanical properties (tensile strength and bending strength), thermal stability, and hydrophobicity of MFP. The changes in the surface composition, chemical structure, crystallinity, and microstructure of MFP before and after the extended delignification were also investigated by X-ray photoelectron spectroscopy (XPS), Fourier transform infrared (FTIR) spectroscopy, X-ray diffraction (XRD), and scanning electron microscopy (SEM), respectively. The results can provide theoretical support for research on forming mechanisms and optimization of process conditions for MFP.

EXPERIMENTAL

Materials

The poplar wood chips were separated into fibers by disc refiner after the pre-impregnation with sodium hydroxide solution to obtain the chemi-thermomechanical pulp (CTMP). Most of the lignin on the surface of CTMP fibers was removed through the process of chlorine dioxide bleaching, and then the bleached pulps were used as the raw fiber materials for the following extended delignification treatment. All of the chemicals were purchased from the Sinopharm Chemical Reagent Co., Ltd. (Beijing, China).

The dry raw fiber material (50 g) was mixed with distilled water (1625 mL). The glacial acetic acid (12.5 mL) and sodium chlorite (15 g) were added into a bath with a temperature of 75 °C and remained for 60 min. Additional glacial acetic acid (12.5 mL) and sodium chlorite (15 g) were added once more to maintain the reaction. When the reaction was performed for 60 min after the second addition of chemicals, the pulp was poured into cold water to terminate the reaction. The fibers were repeatedly washed until neutral and were labeled as extended delignification pulp (EP). At the same time, the raw fiber material was fully dispersed in pure distilled water at 75 °C for 120 min to be used as a control group of pulp (CP).

Methods

Morphology and chemical composition

The dimensions of fibers were observed by a BX53 biological microscope (Olympus Corporation, Tokyo, Japan), and the total number of observed fibers for each group of samples was 600. Fiber cell wall thickness was measured by the cross-section of the fiber in the SEM, and the number of fibers measured for each set of samples was 12. The mean comparison between two groups with the Z-test method at $\alpha = 0.05$ was performed with SAS statistical software (Version 9.4, SAS institute Inc., Cary, NC, USA)

The holocellulose, α-cellulose, and Klason lignin content were determined according to ASTM standards D1104-56 (1971), ASTM D1103-60 (1971), and ASTM D1106-96 (1996), respectively. The pentosan content was determined according to TAPPI T223 CM-2010 (2010). The yields were obtained based on the ratio of the oven-dry weights of the CP or EP to the original weight of the raw fiber material.

Preparation of MFP

The EP was molded using the ZT7-01 molding equipment (Xingping Zhongtong Test Equipment Co., Ltd., Xingping, China). Pre-compaction and hot-pressing processes

were conducted on the ZG-20T pressure machine (Dongguan Zhengyong Electronic Mechanical Ltd., Dongguan, China).

The initial moisture content of samples before hot-pressing was adjusted to 75%. The hot-pressing process was performed under 8 MPa and at 170 °C for 20 min. The obtained samples of MFP (800 g•m^{-2}) were labeled as the extended delignification samples (ES). Under the same molding process mentioned above, the samples of MFP made from CP were labeled as the control group samples (CS).

Mechanical properties of MFP

The density was determined according to ISO 534 (2011). Block samples with sizes of 150 mm × 12 mm and 100 mm × 25 mm were cut for the tensile and bending tests, respectively. The mechanical strength was tested by the CMT5504 universal strength testing machine (Shenzhen SANS Testing Machine Co., Ltd., Shenzhen, China) according to ISO 527-3 (1995) and ISO 178 (2010) standards. The average value of eight measurements in each group of samples was reported as the results.

Characterizations of MFP

Data from the XPS were measured by a Thermo Fisher Scientific K-Alpha X-ray photoelectron spectrometer system with an Al Ka X-ray source (East Grinstead, UK). High-resolution spectrum of the C1s region from 280 eV to 300 eV was collected. Deconvolution of the overlapping peaks was performed *via* the XPS Peak Fitting Program (Thermo Fisher Scientific, XPSPEAK41, East Grinstead, UK). Samples were placed into the Soxhlet and extracted for 8 h with acetone to remove most of the extractives on the fiber surface before the XPS determination (Liu *et al.* 2016).

The FTIR spectra were obtained from a Fourier transform infrared instrument (Frontier, PerkinElmer, Foster, CA, USA). The samples were pelletized with KBr powder. Each spectrum was recorded in the range from 4000 cm^{-1} to 400 cm^{-1}.

The XRD patterns were measured with an X-ray diffractometer (D/max 2200, Rigaku, Tokyo, Japan) using Ni-filtered Cu Kα radiation (λ = 1.5406 Å) at 40 kV and 30 mA. Scattered radiation was detected in the range of 2θ = 5° to 40° at a scan rate of 2°/min. The crystallinity index (CI) was calculated from the heights of the 200 peak (I_{200}, 2θ = 22.6°) and the intensity minimum between the 200 and 110 peaks (I_{am}, 2θ = 18 °) using the Segal method in Eq. 1, where I_{200} represents both crystalline and amorphous material (a.u.) and I_{am} represents the amorphous material (a.u.).

$$C_I(\%) = \left(1 - \frac{I_{am}}{I_{200}}\right) \times 100 \quad (1)$$

A FEI Quanta-200 environment (FEI Company, Golden, Colorado, USA) scanning electron microscope was used. Specimens were coated with gold before observation (Yongzhi Cui, Harbin, China). Cross-sections were obtained using a Feather Microtome blade. Inner surfaces were observed using the hand-torn samples.

Thermogravimetric analysis (TGA) was performed using a differential scanning calorimeter (Diamond DSC, PerkinElmer, Waltham, MA, USA) at the temperature range of 25 °C to 450 °C and the heating rate of 10 °C /min under nitrogen atmosphere.

Water contact angle was measured by an OCA20 contact angle analyzer (Data Physics Co., Filderstadt, Germany), and the average value of five measurements at different places was reported as the result.

RESULTS AND DISCUSSION

Fiber Morphology and Chemical Composition

Extended delignification can cause changes in fiber morphology and chemical composition, which in turn affects the performance of MFP. The average values of the fiber dimensions are shown in Table 1.

Table 1. Average of Fiber Dimensions

Samples	Length (μm)	Z-test	Diameter (μm)	Z-test	Aspect Ratio	Z-test	Cell Wall Thickness (μm)	Z-test
CP	647.5	A	16.9	A	39.6	A	2.76	-
EP	653.0	A	16.4	B	40.6	A	2.76	-
Note: Means with the different letter are significantly different at α = 0.05								

As shown, there were no significant differences in the length, aspect ratio, and cell wall thickness, only for the diameter. After the extended delignification, the diameter of fibers decreased from 16.9 μm to 16.4 μm. The dried cellulose microfibrils were more compact under the action of hydrogen bonds, resulting in a reduced fiber diameter after the extended delignification. At the same time, the removal of residual lignin gave greater microfibril degrees of freedom and fiber softness, which led to greater deformation of the fibers under the hot-press molding process. Therefore, single fiber diameter changes could not directly predict the change in the inter-fiber bonding area in the fiber material. Table 2 shows the fiber yields and main chemical compositions of CP and EP.

Table 2. Fiber Yields and Main Chemical Composition

Sample	Yield (%)	Chemical Compositions (%)				Pentosan in Holocellulose (%)
		Holocellulose	α-cellulose	Pentosan	Lignin	
CP	96.4	86.7	57.7	16.5	5.8	19.0
EP	88.5	93.4	62.2	17.4	0.02	18.7

As shown in Table 2, the EP fiber yield was reduced 8.2% compared to the CP. The lignin content decreased from 5.8% to 0.02% and the holocellulose content increased from 86.7% to 93.4% after the extended delignification, indicating an obvious change in fiber composition. The extended delignification led to a noticeable increase in the amount of cellulose represented by α-cellulose. The content of pentosan in the holocellulose decreased from 19.0% to 18.7%, indicating that the extended delignification caused a certain degree of degradation of hemicellulose, so that the content of pentosan in the fibers did not obviously increase.

Surface Chemical Composition of MFP

X-ray photoelectron spectroscopes provide quantitative information of different bonded carbon atoms on the MFP surface besides the chemical composition (Liang *et al*. 2014), as shown in Fig. 1 and Table 3. Carbon (approximately 285 eV) and oxygen (approximately 532 eV) were the main elements detected in the XPS survey scan, and a small amount of nitrogen (approximately 399 eV) was also found.

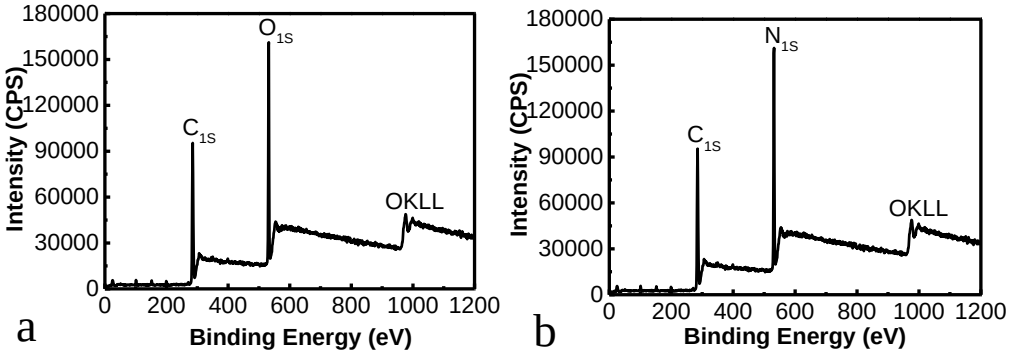

Fig. 1. Survey spectra of samples: a CS; b ES

Due to the removal of acetone-extracted extractives, the increase in the O/C ratio can represent a higher carbohydrate concentration on the material surface (Johansson and Campbell 1999). After the extended delignification, the lignin content in the fiber decreased from 5. 8% to 0.02% (Table 2), while the O/C value of the fiber surface did not change substantially. This illustrated that the residual lignin removed was mainly found in the interior of the fiber and the main chemical composition of the fiber surface was carbohydrates. Therefore, the O/C value was maintained at 0.53 before and after the extended delignification, which was consistent with Gellerstedt and Gatenholm (1999).

Table 3. Results of Material Surface Analysis by XPS

Sample	Atomic Concentration (%)			O/C	Atomic Concentration (%)			C1/C2
	C	O	N		C1	C2	C3	
CS	64.26	34.15	1.59	0.53	34.88	51.06	14.06	0.68
ES	64.04	34.09	1.87	0.53	35.12	49.93	14.79	0.70

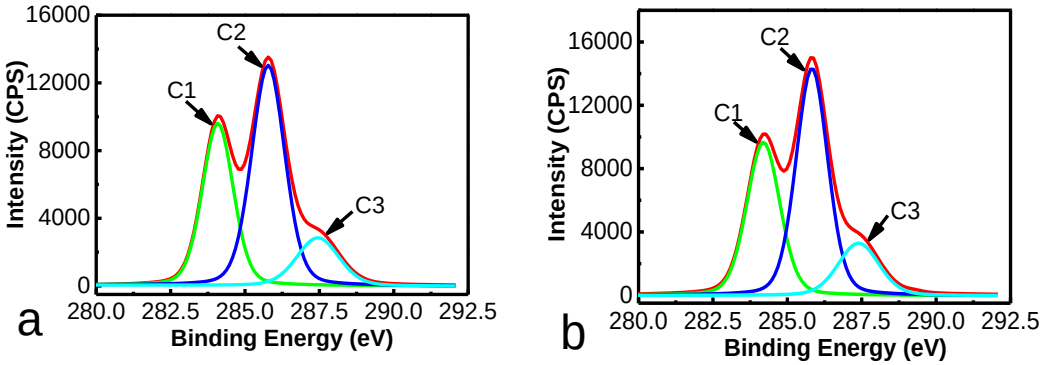

Fig. 2. C1s spectra of samples: a CS; b ES

The high-resolution carbon spectra further highlighted the differences between the CS and ES. The carbon signal can be resolved into four sub-peaks: C1 corresponds to C–C or C–H; C2 refers to the C–O; C3 corresponds to C=O or O–C–O; C4 refers to O–C=O (Edgar and Gray 2003). Lignin in the pulp fiber was treated with sodium chlorite and the degraded products included hexadienedioic acid derivatives, benzoquinones, *etc*.

As shown in Fig. 2, there was no C4 detected, which further indicated that the fiber surface was mainly composed of cellulose and hemicellulose. The relative content of the three kinds of bonded carbon atoms did not change obviously before and after the extended delignification, which indicates that the removal of the residual lignin had no significant effect on the structure and composition of carbohydrates on the fiber surface.

Chemical Composition and Structure of MFP

Fourier transform infrared spectroscopy is an appropriate technique to trace the changes in the chemical structure of the material after extended delignification. Figure 3 shows the FTIR spectra of CS and ES.

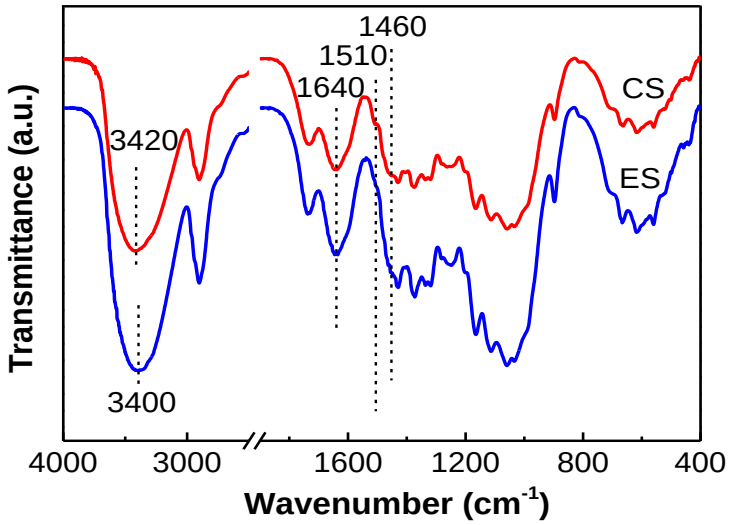

Fig. 3. FTIR spectra of the (a) CS and (b) ES

As shown in Fig. 3, there were no drastic changes in the functional groups of the material during the extended delignification. The 1640 cm^{-1} peak in the CS was associated with the H–O–H stretching vibration of absorbed water in carbohydrates. This peak was still observed in ES, and the intensity slightly increased, which indicated a larger hygroscopicity for ES (Popescu *et al*. 2007).

The 1510 cm^{-1} and 1460 cm^{-1} shoulder peaks in CS represent aromatic ring vibration and C–H deformation vibration of lignin, respectively (Sain and Panthapulakkal 2006). The intensity of these peaks disappeared in ES, which was attributed to the removal of lignin. The OH bonds for cellulose I comprise of two intramolecular links, namely O(2)H•••O(6) bonding (at 3460 cm^{-1} to 3405 cm^{-1}) and O(3)H•••O(5) bonding (at 3375 cm^{-1} to 3340 cm^{-1}) and one intermolecular link, O(6)H•••O(3′) bonding (at 3310 cm^{-1} to 3230 cm^{-1}) (El *et al*. 2017).

After the extended delignification, the OH bonds absorption peak in the region of 3650 cm^{-1} to 3000 cm^{-1} became broader and the wavenumber of OH bonds absorption peak shifted from 3420 cm^{-1} to 3400 cm^{-1}. This indicates that the relative content of intermolecular hydrogen bonds increased, which improves the inter-fiber hydrogen bonding force and the bonding strength among fibers (Schwanninger *et al*. 2004).

X-ray Diffraction Analysis of MFP

The crystallinity of the fibers is closely related to the mechanical properties of MFP. In general, the mechanical strength of the fiber molded material will increase as the crystallinity increases. The XRD patterns and the crystallinity indexes of CS and ES are given in Fig. 4.

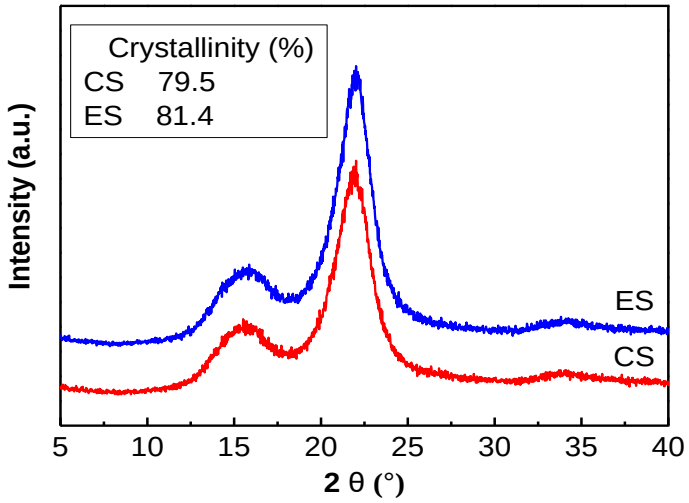

Fig. 4. X-ray diffactograms of CS and ES

It can be observed that the XRD patterns showed nearly consistent diffraction peak positions before and after the extended delignification. This consistency revealed the presence of main diffraction peaks of cellulose at 2θ values of 16° (110) and 22° (200) for CS and ES, corresponding to a typical cellulose I structure, and indicated that the extended delignification did not change the crystalline structure of the fibers. The crystallinity index of the material increased from 79.5% to 81.4% after the extended delignification, mainly due to the removal of residual lignin and the degradation of small amounts of hemicellulose in the amorphous region. In addition, more hydrogen bonds were formed with the exposed hydroxyl groups on the microfibrils inside the crystalline regions and amorphous areas after the extended delignification. These additional hydrogen bonds caused more microfibrils in amorphous areas to move closer to the crystalline regions and to become aligned (Agarwal *et al*. 2017), so that the crystallinity index of the material increases. This was conducive to the improvement of mechanical properties and thermal stability of the material (Nair and Yan 2015; Kian *et al*. 2017).

Micro-morphology Analysis of MFP

To understand the micro morphology changes of the material during the extended delignification, the SEM micrographs of the material surface, cross-section, and inner surface were analyzed and are illustrated in Fig. 5.

As shown in Figs. 5a and 5b, the structure of the ES fiber was further destroyed compared to the CS under the hot-press molding process, and the fibers were completely fused together in a form similar to the adhesive, which showed increased inter-fiber contact area, reduced surface holes, and increased binding compactness. These were clearly beneficial to increasing the inter-fiber bond strength and resulted in an increased tensile strength, which was consistent with the tensile test results.

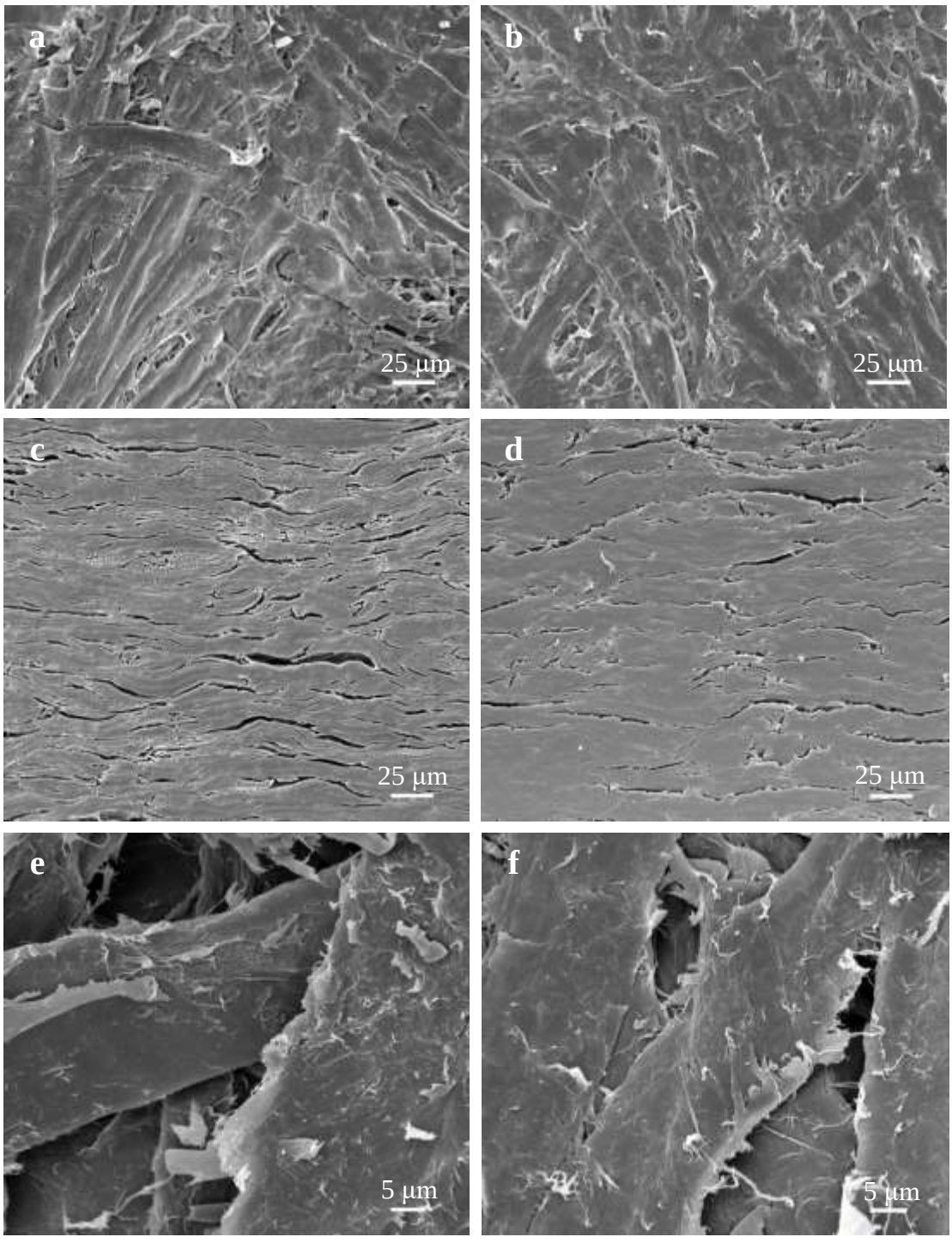

Fig. 5. SEM micrographs of the outer surface (a: CS, b: ES), cross-section (c: CS, d: ES), and inner surface (e: CS, f: ES)

As shown in Figs. 5c and 5d, the fiber cell lumina in the material were completely compacted both before and after the extended delignification, and similar cracks occurred between the fibers due to the existence of local stress. The bending strength of MFP is directly related to the compactness of fiber cell lumina and the state of inter-fiber cracks

(Sinha and Panigrahi 2009), so that there was no obvious change in the bending strength before and after the extended delignification.

As shown in Figs. 5e and 5f, some fiber surfaces exposed regularly arranged microfibrils with an angle approximately 50° to 70°, and the other fibers were covered with hemicellulose, showing a relatively smooth surface in CS and ES. However, the looser arrangement of microfibrils and more uneven scale-like structures were found on the fiber surface in ES compared to CS, which was beneficial for the hydrogen bonding and mechanical locking among fibers.

Physical and Mechanical Properties of MFP

Mechanical strength is an important index to characterize the properties of MFP. The materials' densities and mechanical strengths before and after the extended delignification are shown in Table 4.

Table 4. Density and Mechanical Strength of MFP

Sample	Density ($g \cdot cm^{-3}$)	Tensile Strength (mPa)	Breaking Tensile Strain (%)	Bending Strength (mPa)	Flexural Strain at Bending Strength (%)
CS	1.065	51.13	0.85	126.70	3.92
ES	1.058	64.23	0.99	127.32	4.13

As shown in Table 4, the density slightly decreased, the tensile strength was noticeably improved, and the bending strength had a slight change after the extended delignification. The density decreased 0.7% and the tensile strength increased 25.6% after the removal of residual lignin. The rigid lignin polymer molecules were removed from microfibrils after the extended delignification. This removal generated more loose space within the fibers and caused greater softness and deformation due to the hot-press molding process, so that the tensile strength was greatly improved. The fiber cell lumen in material was compacted both before and after the extended delignification due to the removal of lignin on the fiber surface, and thus the fiber had a similar stiffness and the bending strength of material had no obvious change.

Thermostability Analysis of MFP

Extended delignification may lead to a change in the thermal properties of MFP. The thermogravimetric (TG) and derivative thermogravimetric (DTG) curves of CS and ES are shown in Fig. 6.

As shown in Fig. 6, weight loss was observed in both CS and ES from 26 °C to 115 °C, which corresponded to the evaporation of moisture bound loosely to the fiber surface and the chemisorbed water bound inside the fiber (Jc *et al*. 2016). The presence of absorbed water was also detected by the FTIR characteristic peak at 1640 cm^{-1}. The CS started to degrade at 242 °C with a major decomposition peak at 347 °C, revealed in the DTG curve. For the ES, the onset thermal decomposition (T_{on}) shifted to a higher temperature of 250 °C, with the maximum rate of degradation temperature (T_{max}) at 350 °C. This finding indicated that the extended delignification treatment could eventually enhance the thermal-stability of MFP due to the removal of residual lignin and the degradation of some hemicellulose, as well as the higher crystallinity of cellulose (Du *et al*. 2016). This reasoning agreed well with the XRD results. Similar thermal degradation results were also reported by Chen *et al.* (2016). The residual mass of CS

was approximately 21.6% at 445 °C, which was higher than that of ES. This can be explained by the presence of some non-degraded lignin under that temperature (Vänskä *et al*. 2016).

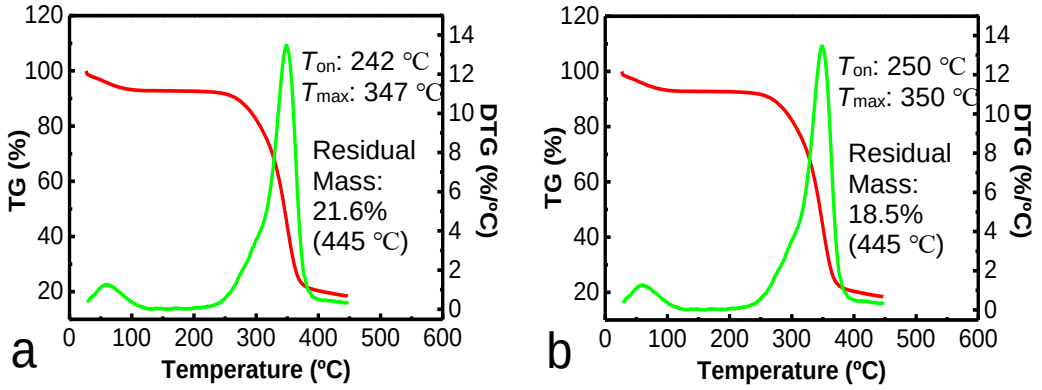

Fig. 6. Thermogravimetric analysis of (a) CS and (b) ES

Hydrophobic Property Analysis of MFP

The water contact angle is an effective method to evaluate the surface hydrophobicity of the material. Figure 7 shows the water contact angles of MFP before and after the extended delignification treatment at the contact time of 60 s.

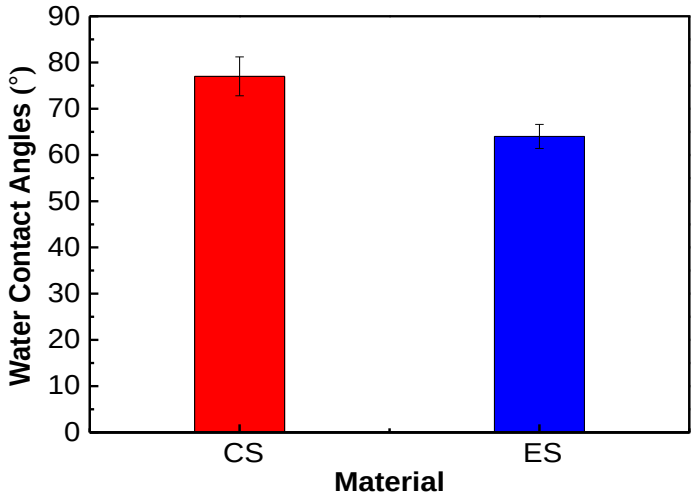

Fig. 7. Water contact angles of the CS and ES

As shown in Fig.7, the water contact angle decreased from 77° to 64° after the extended delignification, which indicated a decrease of the material hydrophobicity. As is well known, there are two basic ways to improve the hydrophobicity of a surface: (1) by increasing the surface roughness and (2) by lowering the surface energy (Peng *et al*. 2016). For cellulose fibers, the relative content of hydroxyl radical characterized by the C1/C2 ratio is one of the important factors that affects the surface energy (Liu *et al*. 2016). Interestingly, a slight difference was found between the C1/C2 values before and

after the extended delignification in the XPS result. The SEM observations showed a rougher surface for CS, while the ES appeared to have a smoother surface. This may be explained by the decrease in the hydrophobicity of the material after the extended delignification.

CONCLUSIONS

1. After the removal of residual lignin, the content of lignin decreased from 5.8% to 0.02% with a noticeable increase in cellulose content and a small amount of hemicellulose degradation. No significant changes were found in the fiber morphology dimensions, except for the reduced fiber diameter.
2. The removed residual lignin existed only within the fibers, and the extended delignification had no significant effect on the fiber surface carbohydrates. The residual lignin had been removed and the relative content of intermolecular hydrogen bonds in cellulose increased after the extended delignification. The crystallinity index of the material increased from 79.5% to 81.4% after the extended delignification. The fibers were completely fused together in a form similar to an adhesive with increased inter-fiber contact area, but slight changes were found in the material cross-section after the extended delignification.
3. The density slightly decreased, the bending strength had no obvious change, and the tensile strength increased 25.6% after the extended delignification. The thermal stability increased as the onset thermal decomposition temperature increased from 242 °C to 250 °C and the maximum rate of degradation temperature increased from 347 °C to 350 °C after the extended delignification. However, the hydrophobicity was reduced as the water contact angle decreased from 77° to 64° after the extended delignification. Although the removal of residual lignin resulted in a slight decrease in the hydrophobicity of the molded fiber product, it could significantly improve the mechanical properties and thermal stability, which was beneficial to expand the application range and service life of the molded fiber product.

ACKNOWLEDGMENTS

The authors gratefully acknowledge the financial support from the National Key R&D Program of China (2017YFD0601004) and the Fundamental Research Funds for Central Universities (Harbin, China) (2572016AB69) for this study.

REFERENCES CITED

Agarwal, U. P., Ralph, S. A., Baez, C., Reiner, R. S., and Verrill, S. P. (2017). "Effect of sample moisture content on XRD-estimated cellulose crystallinity index and crystallite size," *Cellulose* 24(5), 1971-1984. DOI: 10.1007/s10570-017-1259-0

ASTM D1103-60 (1971). "Standard test method for alpha-cellulose in wood," ASTM International, West Conshohocken, PA.

ASTM D1104-56 (1971). "Standard test method for holocellulose in wood," ASTM International, West Conshohocken, PA.

ASTM D1106-96 (1996). "Standard test method for acid-insoluble lignin in wood," ASTM International, West Conshohocken, PA.

Baptista, C., Robert, D., and Duarte, A. P. (2008). "Relationship between lignin structure and delignification degree in *Pinus pinaster* kraft pulps," *Bioresource Technol.* 99(7), 2349-2356. DOI: 10.1016/j.biortech.2007.05.012

Brebu, M., Tamminen, T., and Spiridon, I. (2013)."Thermal degradation of various lignins by TG-MS/FTIR and Py-GC-MS," *J. Anal. Appl. Pyrol.* 104(11), 531-539. DOI: 10.1016/j.jaap.2013.05.016

Chen, Y. W., Lee, H. V., Juan, J. C., and Phang, S. M. (2016)."Production of new cellulose nanomaterial from red algae marine biomass *Gelidium elegans*," *Carbohydr. Polym.* 151, 1210-1219. DOI: 10.1016/j.carbpol.2016.06.083

Cho, B. U., Ryu, J. Y., and Song, B. K. (2009). "Factors influencing deflaking kinetics in repulping to produce molded pulp," *J. Ind. Eng. Chem.* 15(1), 119-123. DOI: 10.1016/j.jiec.2008.08.003

Domínguez, J. C., Oliet, M., Alonso, M. V., Gilarranz, M. A., and Rodríguez, F. (2008). "Thermal stability and pyrolysis kinetics of organosolv lignins obtained from *Eucalyptus globulus*," *Ind. Crop Prod.* 27(2), 150-156. DOI: 10.1016/j.indcrop.2007.07.006

Du, H., Liu, C., Mu, X., Gong, W., Lv, D., Hong, Y., Si, C., and Li, B. (2016). "Preparation and characterization of thermally stable cellulose nanocrystals *via* a sustainable approach of $FeCl_3$-catalyzed formic acid hydrolysis," *Cellulose* 23(4), 2389-2407. DOI: 10.1007/s10570-016-0963-5

Edgar, C. D., and Gray, D. G. (2003). "Smooth model cellulose I surfaces from nanocrystal suspensions," *Cellulose* 10(4), 299-306. DOI: 10.1023/A:1027333928715

El, O. A., Msahli, S., and Sakli, F. (2017). "In-depth study of agave fiber structure using Fourier transform infrared spectroscopy," *Carbohydr. Polym.* 164, 242-248. DOI: 10.1016/j.carbpol.2017.01.091

Ferrer, A., Quintana, E., Filpponen, I., Solala, I., Vidal, T., Rodríguez, A., Laine, J., and Rojas, O. J. (2012). "Effect of residual lignin and heteropolysaccharides in nanofibrillar cellulose and nanopaper from wood fibers," *Cellulose* 19(6), 2179-2193. DOI: 10.1007/s10570-012-9788-z

Gällstedt, M., and Hedenqvist, M. S. (2006). "Packaging-related mechanical and barrier properties of pulp–fiber–chitosan sheets," *Carbohydr. Polym.* 63(1), 46-53. DOI: 10.1016/j.carbpol.2005.07.024

Gellerstedt, F., and Gatenholm, P. (1999). "Surface properties of lignocellulosic fibers bearing carboxylic groups," *Cellulose* 6(2), 103-121. DOI: 10.1023/A:1009239225050

ISO 178 (2010). "Plastics - Determination of flexural properties," International Organization for Standardization, Geneva, Switzerland.

ISO 527-3 (1995). "Plastics - Determination of tensile properties - Part 3: Test conditions for films and sheets," International Organization for Standardization, Geneva, Switzerland.

ISO 534 (2011). "Paper and board - Determination of thickness, density and specific volume," International Organization for Standardization, Geneva, Switzerland.

Jc, C. S., George, N., and Narayanankutty, S. K. (2016). "Isolation and characterization of cellulose nanofibrils from arecanut husk fibre," *Carbohydr. Polym.* 142, 158-166. DOI: 10.1016/j.carbpol.2016.01.015

Johansson, L. S., and Campbell, J. M. (1999). "Evaluation of surface lignin on cellulose fibers with XPS," *Appl. Surf. Sci.* 144(98), 92-95. DOI: 10.1016/S0169-4332(98)00920-9

Kadla, J. F., and Chang, H. M. (2002). "Reactions of lignin with cyanamide activated hydrogen peroxide. Part 3. The degradation of pine kraft lignin," *Holzforschung* 56(1), 76-84. DOI: 10.1515/HF.2002.013

Kian, L. K., Jawaid, M., Ariffin, H., and Alothman, O. Y. (2017). "Isolation and characterization of microcrystalline cellulose from roselle fibers," *Int. J. Biol. Macromol.* 103, 931-940. DOI: 10.1016/j.ijbiomac.2017.05.135

Korai, H., Kojima, Y., and Suzuki, S. (2015). "Bending strength and internal bond strength of wood-based boards subjected to various exposure conditions," *J. Wood Sci.* 61(5), 1-10. DOI: 10.1007/s10086-015-1494-7

Laurichesse, S., and Avérous, L. (2014). "Chemical modification of lignins: Towards biobased polymers," *Prog. Polym. Sci.* 39(7), 1266-1290. DOI: 10.1016/j.progpolymsci.2013.11.004

Liang, K., Shi, S. Q., and Wang, G. (2014). "Effect of impregnated inorganic nanoparticles on the properties of the kenaf bast fibers," *Fibers* 2(3), 242-254. DOI: 10.3390/fib2030242

Lin, B. P., He, B. H., and Zhao, G. L. (2011). "The impact of lignin content on paper physical strength of CTMP," *Advanced Materials Research* 236-238, 1242-1245. DOI: 10.4028/www.scientific.net/AMR.236-238.1242

Liu, Y. Y., Liu, M. R., Li, H. L., Li, B. Y., and Zhang, C. H. (2016). "Characteristics of high yield pulp fibers by xylanase treatment," *Cellulose* 23(5), 1-9. DOI: 10.1007/s10570-016-1032-9

Miletzky, A., Fischer, W. J., Czibula, C., Teichert, C., Bauer, W., and Schennach, R. (2015). "How xylan effects the breaking load of individual fiber–fiber joints and the single fiber tensile strength," *Cellulose* 22(1), 849-859. DOI: 10.1007/s10570-014-0532-8

Nair, S. S., and Yan, N. (2015). "Effect of high residual lignin on the thermal stability of nanofibrils and its enhanced mechanical performance in aqueous environments," *Cellulose* 22(5), 3137-3150. DOI: 10.1007/s10570-015-0737-5

Obradovic, J., Wondraczek, H., Fardim, P., Lassila, L., and Navard, P. (2014). "Preparation of three-dimensional cellulose objects previously swollen in a DMAc/LiCl solvent system," *Cellulose* 21(6), 4029-4038. DOI: 10.1007/s10570-014-0403-3

Peng, L., Meng, Y., and Li, H. (2016). "Facile fabrication of superhydrophobic paper with improved physical strength by a novel layer-by-layer assembly of polyelectrolytes and lignosulfonates-amine," *Cellulose* 23(3), 1-13. DOI: 10.1007/s10570-016-0910-5

Poletto, M., Zattera, A. J., Forte, M. M. C., and Santana, R. M. C. (2012). "Thermal decomposition of wood: Influence of wood components and cellulose crystallite size," *Bioresource Technol.* 109(1), 148-153. DOI: 10.1016/j.biortech.2011.11.122

Popescu, C. M., Popescu, M. C., Singurel, G., Vasile, C., Argyropoulos, D. S., and Willfor, S. (2007). "Spectral characterization of eucalyptus wood," *Appl. Spectrosc.* 61(11), 1168-1177. DOI: 10.1366/000370207782597076

Rojo, E., Peresin, M. S., Sampson, W. W., Hoeger, I. C., Vartiainen, J., Laine, J., and Rojas, O. J. (2015). "Comprehensive elucidation of the effect of residual lignin on the physical, barrier, mechanical and surface properties of nanocellulose films," *Green Chem.* 17(3), 1853-1866. DOI: 10.1039/C4GC02398F

Sain, M., and Panthapulakkal, S. (2006). "Bioprocess preparation of wheat straw fibers and their characterization," *Ind. Crop Prod.* 23(1), 1-8. DOI: 10.1016/j.indcrop.2005.01.006

Schwanninger, M., Rodrigues, J. C., Pereira, H., and Hinterstoisser, B. (2004). "Effects of short-time vibratory ball milling on the shape of FT-IR spectra of wood and cellulose," *Vib. Spectrosc.* 36(1), 23-40. DOI: 10.1016/j.vibspec.2004.02.003

Sinha, E., and Panigrahi, S. (2009). "Effect of plasma treatment on structure, wettability of jute fiber and flexural strength of its composite," *J. Compos. Mater.* 43(17),1791-1802. DOI: 10.1177/0021998309338078

TAPPI T223 (2010). "Pentosans in wood and pulp," TAPPI Press, Atlanta, GA.

Vänskä, E., Vihelä, T., Peresin, M. S., Vartiainen, J., Hummel, M., and Vuorinen, T. (2016). "Residual lignin inhibits thermal degradation of cellulosic fiber sheets," *Cellulose* 23(1), 199-212. DOI: 10.1007/s10570-015-0791-z

Wang, Q. L., Xiao, S. L., Yue, J. Q., and Lu, X. Z. (2017). "Moisture transfer process of hot-press molding of overloaded molded fiber material," *Packaging Engineering* 38(9), 96-101. DOI: 10.19554/j.cnki.1001-3 563.2017.09.019

Wen, J. L., Sun, S. L., Yuan, T. Q., Xu, F., and Sun, R. C. (2013). "Structural elucidation of lignin polymers of eucalyptus chips during organosolv pretreatment and extended delignification," *J. Agr. Food Chem.* 61(46), 11067-11075. DOI: 10.1021/jf403717q

Yang, G. Y., Jin, Y. U., Zhao, Y., and Xiang, Y. (2005). "Effect of vacuum suction/ filtering on quality of disposal pulp molded food wares," *Vacuum* 42(3), 49-50. DOI: 10.13385/j.cnki.vacuum.2005.03.013

Zhang, S. Y., Fei, B. H., Yan, Y. U., and Cheng, H. T. (2012). "Influence of lignin content on tensile properties of single wood fiber," *Journal of Beijing Forestry University* 34(1), 131-134. DOI: 10.13332/j.1000-1522.2012.01.008

Zhang, X., Zhao, Z., Ran, G., Liu, Y., Liu, S., Zhou, B., and Wang, Z. (2013). "Synthesis of lignin-modified silica nanoparticles from black liquor of rice straw pulping," *Powder Technol.* 246(9), 664-668. DOI: 10.1016/j.powtec.2013.06.034

Article submitted: August 16, 2017; Peer review completed: October 29, 2017; Revised version received: November 1, 2017; Accepted: November 2, 2017; Published: November 3, 2017.
DOI: 10.15376/biores.13.1.71-85